Isobaric to Isentropic Interpolation Errors and Implication to Potential Vorticity Analysis

BARUCH ZIV AND PINHAS ALPERT

Department of Geophysics and Planetary Sciences, Raymond and Beverly Sackler Faculty of Exact Sciences, Tel Aviv University, Tel Aviv, Israel

(Manuscript received 1 July 1993, in final form 1 December 1993)

ABSTRACT

Different common interpolation methods have been used for transformation of atmospheric variables from pressure levels into isentropic levels. The accuracy of the derived variables depends both on the specific interpolation method chosen and on the vertical resolution of the pressure levels. A most sensitive field is $\partial\theta/\partial p$, the stability factor, in which error largely determines also that of the isentropic potential vorticity. Five interpolation methods are compared using radiosonde observations. They are examined through their capability to resolve isentropic profiles of the stability factor as well as the pressure based on data from arbitrary pressure surfaces. Comparison of the results with full resolution data reveals, not unexpectedly, that fine vertical patterns are not resolvable. The methods differ in their ability to resolve patterns found with 10-pressure-level data when applied to only seven levels. However, the method based on the linear θ–p relation is shown to yield larger errors than other methods, such as that based on the linear T–ln$p$ relation. In addition, the advantage of the latter method is clearly demonstrated through isentropic and vertical potential vorticity distribution with ECMWF data.

1. Introduction

In recent years, a major part of data used for atmospheric diagnostics studies came from numerical global prediction models, like those of the National Meteorological Center (NMC) and the European Centre for Medium-Range Forecasts (ECMWF). These data consist of atmospheric variables given at discrete pressure or sigma levels, with limited spatial and temporal resolution. As it is processed and transformed into another coordinate system, like the isentropic system for mesoscale modeling or diagnostic studies, errors are inevitable. A central isentropic variable is the Ertel potential vorticity (PV) on isentropic surfaces under hydrostatic conditions, given by

$$P = -g\eta\frac{\partial\theta}{\partial p}, \tag{1}$$

where P is the PV, g is gravity, p is the pressure, θ is the potential temperature, η is the vertical component of the absolute vorticity derived on isentropic surfaces, and $\partial\theta/\partial p$ is the stability factor (Bleck 1973). Following (1), the PV relative error is

$$\frac{\Delta P}{P} = \frac{\Delta\eta}{\eta} + \frac{\Delta(\partial\theta/\partial p)}{(\partial\theta/\partial p)}, \tag{2}$$

where ΔP, $\Delta\eta$, and $\Delta(\partial\theta/\partial p)$ are the errors in the respective variables. The absolute vorticity error $\Delta\eta$ equals the relative vorticity error $\Delta\zeta$. Taking a 5%–10% error in the wind measurements (Holton 1992; Houghton 1985), $\Delta\zeta \simeq \zeta/10$. If the relative vorticity ζ is assumed to be one order of magnitude smaller than the Coriolis parameter f at midlatitudes (Holton 1992), the relative error in the absolute vorticity η becomes $\Delta\eta/\eta \simeq 0.1\zeta/f \simeq 10^{-2}$. As shown later (sections 4b and 4c), the relative error in the stability factor is about one order of magnitude larger (10^{-1}) and is therefore the dominant contributor to the PV error. The crucial role played by the stability factor necessitates improving the accuracy of its numerical value and of the reliability in its spatial distribution.

Suppose that temperature is given at discrete pressure levels (Fig. 1). In order to calculate the pressure and to derive the stability factor at the isentropic level θ, an interpolation between the potential temperature values at the up and down pressure levels p_u and p_d, respectively, is done. The interpolation methods differ by the assumed relation between potential temperature and pressure within the relevant pressure interval. The aim of this paper is to compare five such methods in their ability to recover the structure of the stability factor (and hence the PV) from data given at discrete pressure levels and to evaluate the dependence on the vertical separation of those levels.

The study is divided into two parts. The quantitative part, based on radiosonde observations, deals with the p–θ relation and the stability parameter. The illustra-

Corresponding author address: Dr. Pinhas Alpert, Department of Geophysics and Planetary Sciences, Raymond and Beverly Sackler Faculty of Exact Science, Tel Aviv University, Tel Aviv, 69978, Israel.

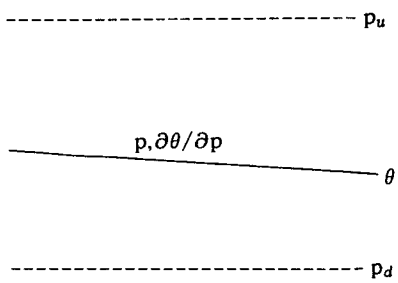

FIG. 1. Pressure levels (dashed lines) and isentropic level (solid line).

tive part includes PV charts both on isentropic surfaces and for vertical cross sections and is based upon ECMWF initialized data. The PV is calculated with the stability factor extracted according to the relevant interpolation method.

Section 2 describes the five interpolation methods, while section 3 demonstrates through isentropic PV distributions the deficiency of one of the methods. Next, section 4 compares the methods with the aid of a collection of radiosonde data. In section 5 isentropic and vertical cross sections of PV distributions are employed for a further evaluation. The last section summarizes the results and discusses their significance.

2. Methods of interpolation

Following are methods that have been used for conversion of atmospheric variables from pressure levels to other coordinate systems. The presentation refers to the isentropic level θ that lies between an upper pressure level p_u and a lower pressure level p_d (Fig. 1) with temperature T_u and T_d and potential temperature θ_u and θ_d, respectively. Each of the following methods relies on some relationship between temperature and pressure within the interval (p_u, p_d).

a. *Linear dependence of potential temperature on pressure*

The stability factor and pressure are given by

$$\frac{\partial\theta}{\partial p} = \frac{(\theta_u - \theta_d)}{(p_u - p_d)}, \tag{3}$$

$$p = p_d + (\theta - \theta_d)\frac{(p_u - p_d)}{(\theta_u - \theta_d)}. \tag{4}$$

Here, all isentropic levels between two adjacent pressure levels have the same stability factor.

This method was used in an isentropic forecasting model by Bleck (1974) for extracting the pressure while the stability factor was calculated through vertical derivatives of the Montgomery streamfunction. Hoskins et al. (1985) and Neeman and Alpert (1990) also used this method for extracting large-scale PV maps using ECMWF data.

b. *Linear dependence of potential temperature on the Exner function*

The Exner function π is given by

$$\pi \equiv c_p\left(\frac{p}{p_0}\right)^{\kappa}, \tag{5}$$

where p_0 is the reference pressure of 1000 hPa, c_p is the specific heat at constant pressure, and $\kappa = R/c_p$, where R is the gas constant. Equation (5) implies that potential temperature varies linearly with p^{κ}. Considering an isentropic level θ that lies between the above-mentioned pressure levels, the pressure and stability factor are

$$p = \left[(\theta - \theta_d)\left(\frac{p_u^{\kappa} - p_d^{\kappa}}{\theta_u - \theta_d}\right) + p_d^{\kappa}\right]^{1/\kappa} \tag{6}$$

$$\frac{\partial\theta}{\partial p} = \frac{\kappa\pi(\theta_u - \theta_d)}{p(\pi_u - \pi_d)}. \tag{7}$$

This method was used by Bleck (1973), when extracting isentropic variables out of radiosonde data and more recently by Davis and Emanuel (1991) for calculating quasigeostrophic PV from NMC gridded data.

c. *Linear dependence of temperature on lnp*

Here, the temperature as a function of pressure is

$$T = A + B\ln p;$$

$$A = T_d - \frac{T_u - T_d}{\ln(p_u/p_d)}\ln p_d; \quad B = \frac{T_u - T_d}{\ln(p_u/p_d)}. \tag{8}$$

Hence, the potential temperature and stability factor are

$$\theta = \frac{Ac_p}{\pi} + \frac{Bc_p}{\pi}\ln p, \tag{9}$$

$$\frac{\partial\theta}{\partial p} = -\frac{c_p}{p\pi}(A\kappa + B\kappa\ln p - B). \tag{10}$$

Here, the pressure is obtained by the Newton–Rapson iteration method solving (9) and using the pressure derived by method (a) as a first guess.

This T–p relation is used by NMC for interpolating sigma-level analysis to constant pressure levels during the postprocessing phase (Hoerling and Sanford 1993).

d. *Linear dependence of temperature on height*

Here, a constant lapse rate between the pressure levels is assumed. This condition, when applied to the hydrostatic equation, yields (Shen et al. 1986)

$$T = T_u\left(\frac{p}{p_u}\right)^{R\Gamma/g}; \quad \Gamma \equiv \frac{T_d - T_u}{z_u - z_d}, \tag{11}$$

where z_u and z_d are the corresponding geopotential heights of the up and down pressure levels. The pressure and the stability factor are given by

$$p = \left(\frac{\theta}{A}\right)^{1/B}, \tag{12}$$

$$\frac{\partial\theta}{\partial p} = BAp^{B-1}, \tag{13}$$

where $A \equiv Tp_0^{\kappa}/p_u^{R\Gamma/g}$ and $B \equiv R(\Gamma g^{-1} - c_p^{-1})$.

This relation was used by Shen et al. (1986) for interpolation of pressure-level data to sigma levels. This is the only method where additional data besides temperature, say the geopotential height, is required.

e. Linear dependence of temperature on p^{κ}

Here, the temperature as a function of pressure is

$$T = T_d + (p^{\kappa} - p_d^{\kappa})\frac{T_u - T_d}{p_u^{\kappa} - p_d^{\kappa}}. \tag{14}$$

Hence, the pressure and stability factor are

$$p = \left\langle \frac{\{p_0^{\kappa}[(T_u - T_d)(p_u - p_d)^{-1}]\} - \theta}{p_0^{\kappa}\{p_d^{\kappa}[(T_u - T_d)(p_u - p_d)^{-1}]\} - T_d} \right\rangle^{-1/\kappa}, \tag{15}$$

$$\frac{\partial\theta}{\partial p} = \kappa p_0^{\kappa}\{[(T_u - T_d)(p_u - p_d)^{-1}]p_d^{\kappa} - T_d\}^{-(1+\kappa)}. \tag{16}$$

This method was used by Schaack et al. (1990) for interpolation of ECMWF pressure level data to isentropic level in order to study the global diabatic heating rates through the isentropic equation of mass continuity.

Main features of the five methods are given in Table 1.

3. PV distributions following method (a)

A convenient way to evaluate the derived PV field qualitatively is to examine its spatial distribution, and particularly the significant features like PV anomalies. Local extremes in PV will be referred to as anomalies. The analysis makes use of ECMWF initialized data, containing three atmospheric variables, two wind components, temperature and geopotential height on the seven pressure levels of 1000, 850, 700, 500, 300, 200, and 100 hPa (e.g., Bengtsson et al. 1982; Hollingsworth et al. 1986; Shaw et al. 1987). The PV extraction follows method (a). Figure 2 shows a series of PV distributions for 0000 UTC 15 December 1986 on the 340-, 330-, and 320-K isentropic surfaces. The 320- and 330-K distributions are quite similar except for small differences in the fine structure. Comparison between the PV distributions on the 330- and 340-K surfaces, however (Figs. 2b and 2a), indicates substantial differences, among which is the existence of a 340-K positive anomaly over the Balkans and the central Mediterranean in Fig. 2a (at about 35°–45°N, 15°–28°E) located above negative anomalies below, at 330 and 320 K. Another difference to be next shown as an inconsistency is in the PV distribution over the Baltic Sea (50°–58°N, 10°–20°E), where a local maximum is found at 340 K only.

An increase in PV with height is expected in the vicinity of the tropopause and throughout the stratosphere, where the isothermal conditions result in a gradual change in the stability factor (e.g., Fig. 1 in Hoskins et al. 1985). Method (a) does not reflect such gradual vertical PV changes, but rather an abrupt change whenever an isentropic surface intersects one of the pressure levels from which the data is taken. The above-mentioned differences between the 330- and 340-K surfaces correspond, indeed, to the pressure distributions over these isentropic surfaces (Fig. 3). The 320 and 330 K are between pressure levels 200 and 300 hPa over most of Europe and the Mediterranean, where most of the significant PV anomalies are located. The 340-K surface also lies between the 200- and 300-

TABLE 1. Features of the five interpolation methods.

Method	Source	T–p relation	θ–p relation	Basic assumption
(a)	Bleck (1974) Hoskins et al. (1985) Neeman and Alpert (1990)	$T = Ap^{\kappa} + Bp^{1+\kappa}$	$\theta = C + Dp$	constant stability factor
(b)	Bleck (1973) Davis and Emanuel (1991)	$T = Ap^{\kappa} + Bp^{2\kappa}$	$\theta = C + Dp^{\kappa}$	constant temperature
(c)	NMC	$T = A + B\ln p$	$\theta = Cp^{-\kappa} + Dp^{-\kappa}\ln p$	approximated version of method (d)
(d)	Shen et al. (1986)	$T = Ap^{\Gamma R/g}$	$\theta = Cp^{-\kappa}p^{\Gamma R/g}$	constant lapse rate
(e)	Schaack et al. (1990)	$T = A + Bp^{\kappa}$	$\theta = Cp^{-\kappa} + D$	dry-adiabatic lapse rate

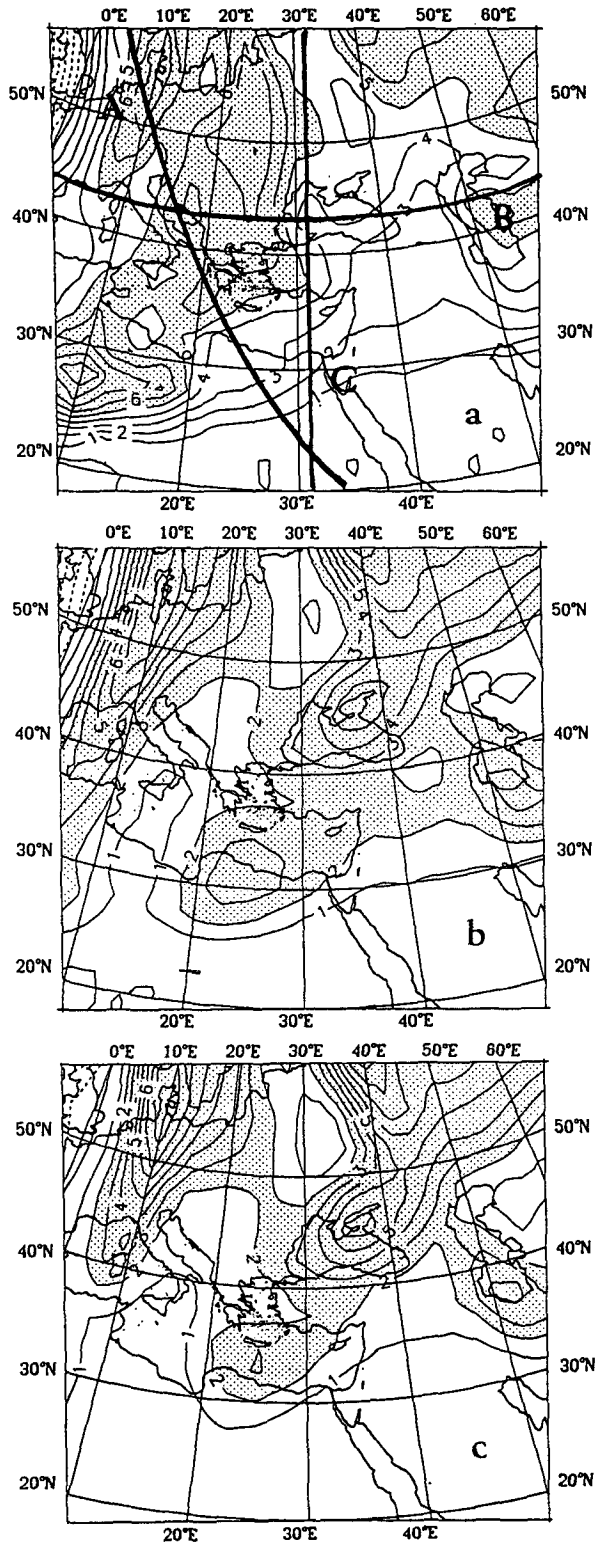

FIG. 2. The (a) 340-K, (b) 330-K, and (c) 320-K PV distributions for 0000 UTC 15 December 1986 in potential vorticity units (PVU) 1 PVU = 10^{-6} m^2 s^{-1} K kg^{-1}) with an interval of 1 PVU. The stability factor is derived using method (a). Values exceeding 2 PVU [5 PVU *in panel (a)*] are shaded. The heavy lines denote the locations of the cross sections shown in Fig. 12.

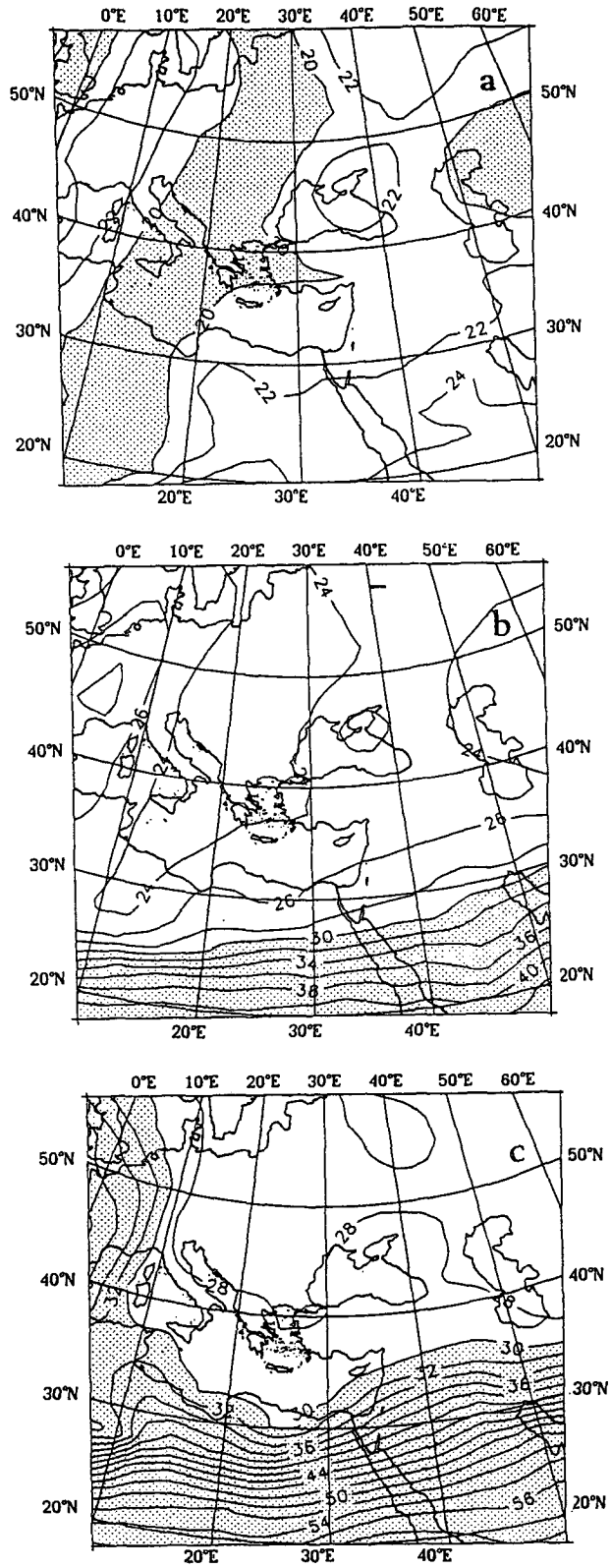

FIG. 3. Pressure distributions with interval of 2 kPa for the same case as in Fig. 2 over the isentropic surfaces: (a) 340 K, areas where pressure is lower than 200 hPa shaded; (b) 330 K, shaded above 300 hPa; and (c) 320 K, shaded above 300 hPa.

hPa pressure levels over most of the region of interest, except for a limited area (shaded in Fig. 3a) covering the central Mediterranean and eastern Europe, where it intersects the 200-hPa pressure level and penetrates above it. This intersection results in an abrupt change in the stability parameter over that region, and hence in the PV field. The aforementioned differences between the isentropic levels will be discussed later as they relate to the choice of interpolation method.

4. Comparison of interpolation methods against radiosonde data

a. Method

The quantitative comparison study is based on raw data taken from sonde observations. Besides being a most reliable source for atmospheric profiles, the radiosondes are free from errors that characterize the output data from forecast models due to the processing and postprocessing procedures. The reported significant points are chosen so that the temperature dependence on log pressure is linear between two successive points according to the international convention of the sonde report (WMO 1988). Thus, when the parameters are computed using method (c) they can serve for reference purposes. The sondes' data are from the international meteorological network covering the area (20°–70°N, 25°W–55°E) for the periods 18–24 January and 16–19 February 1983. In order to get a broad statistical basis, 100 sondes were chosen randomly after excluding those where any superadiabatic layer was detected. The following tests were performed twice, using an independent sample of 100 sondes. Though the results are not identical, the findings are similar.

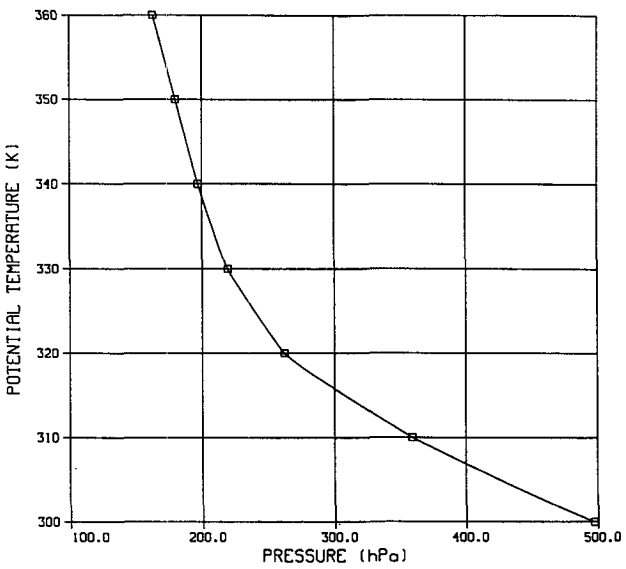

FIG. 4. Average pressure (hPa) on isentropic levels for the 100 sondes' output. Isentropic surfaces lower than 300 K were excluded in order to avoid possible intersection with the earth surface.

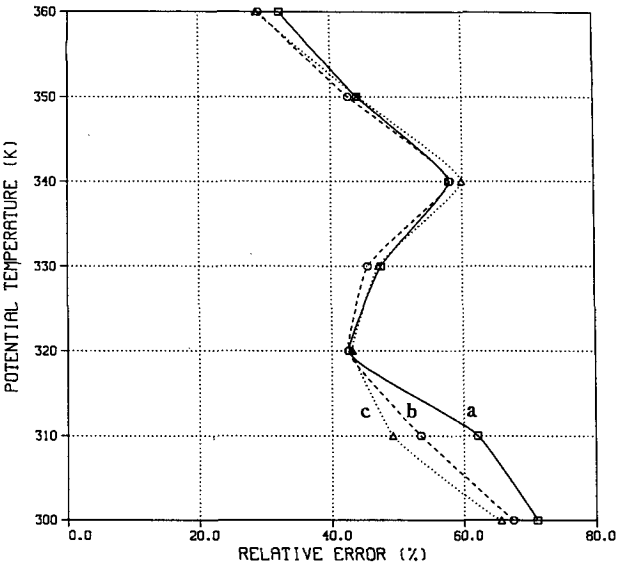

FIG. 5. Relative errors in the stability factor derived by the three methods (a) (solid), (b) (dashed), and (c) (dotted) as compared with 100 sondes' output. Data is given at seven pressure levels with respect to reference values extracted from full data.

The five interpolation methods were employed for each sonde in order to calculate the stability factor and the pressure over seven isentropic levels ranging from 300 to 360 K with 10-K intervals using temperatures at only arbitrarily chosen pressure levels, and then compared to the reference values derived from the full sonde report ("true" value). Denoting the deviation of an interpolated variable, x_i, of a sonde i from its reference "true" value for a certain isentropic j level by $\Delta x_{i,j}$ the relative error ΔX_j for that isentropic level is defined by

$$\Delta X_j = \frac{1}{X_j}\left[\frac{1}{n}\sum_{i=1}^{n}(\Delta x_{i,j})^2\right]^{1/2}, \qquad (17)$$

where X_j is the mean true value of x over all the n sondes for level j.

The relation between pressure and potential temperature is shown by the mean pressure at each isentropic level for these 100 cases (Fig. 4).

b. Stability errors with 7 and 10 pressure levels

The five methods were applied, using 1000, 850, 700, 500, 300, 200, and 100 hPa as the arbitrary pressure levels. The relative errors in the stability factor for methods (a)–(c) are shown in Fig. 5. Method (a) seems to be worst for the lower and upper levels, while method (c) is best at lower isentropic levels, and method (b) is the best at the medium and upper levels. Since the errors of methods (d) and (e) are similar to those of method (c) (within 1%), they are not shown. All methods, however, are quite close to each other with

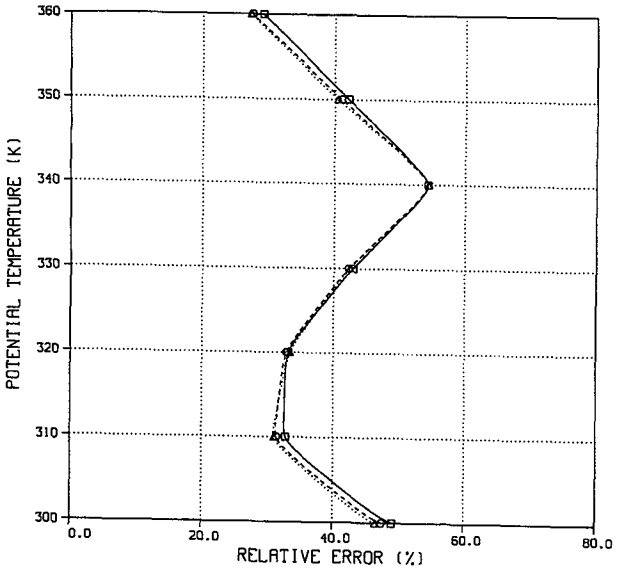

FIG. 6. Same as Fig. 5 but where the stability factor is derived from 10 pressure levels.

relative errors of about 30%–70%. This indicates that the recovering of any fine structure of the stability factor distributions calculated from the seven pressure levels is impractical.

Another test was done using 10 pressure levels of data, including in addition to the 7 above-mentioned levels the 400-, 250-, and 150-hPa surfaces. The results, Fig. 6, still show large relative errors, but about 10%–15% smaller. Here again, method (a) is the worst and method (c) is very close to methods (d) and (e). Methods (b) and (c) are very close to each other, though the latter is a little better. Both experiments are consistent in their implication that sampling of a temperature profile by 7–10 pressure levels produces a relative error of about half, and hence does not enable the recovery of the fine vertical structure of the stability factor. Since the relative error in the stability factor determines the PV relative error, this implies that similar order of magnitude errors may be induced in the derived PV field. Potential vorticity errors of 50% are significant, especially in quantitative studies.

c. *Stability errors in 7 pressure levels against 10 pressure levels*

As one may expect, stability errors obtained in a comparison with radiosondes containing, in general, 20 data levels were found to be large. These errors originate from fine structures in the vertical profiles, which are not captured by lower-resolution data, usually treated as subgrid-scale features when dealing with synoptic systems. Therefore, for synoptic diagnosis it is of interest to examine the capability of the various interpolation methods, applied to 7 levels, to capture subsynoptic features as reflected, for instance, by 10-level data.

Therefore, in the next experiment the reference stability factor was calculated from the radiosonde data using 10 levels as the basis for the reference profile [calculated by method (c)]. The stability factor relative error obtained by methods (a)–(c) applied using data from the 7 pressure levels is shown in Fig. 7. The errors in this case are about 40%–50% at lower levels and 10%–20% at upper levels. The gap between the different methods is quite significant. Here, again, method (a) is the worst and method (c) is the best. The errors of methods (c)–(e) do not differ by more than 1%. When this experiment was repeated with reference values calculated by method (b) the methods (c)–(e) remained superior, although the gap between them and method (b) has been reduced (not shown).

d. *Pressure errors*

To reexamine the skill of the various interpolation methods, they were used to compute the pressure at the isentropic levels with data from the seven pressure levels. The reference pressure for each sonde was computed from the raw data by method (c) for the above-mentioned arguments. The results shown in Fig. 8 confirm our earlier finding regarding the hierarchy among the methods, except for the lower levels, where no significant difference was found between them. Here, again, no significant difference was found among methods (c), (d), and (e).

e. *θ interpolation between pressure levels*

The skill differences among the different interpolation methods were hardly detected when using exact

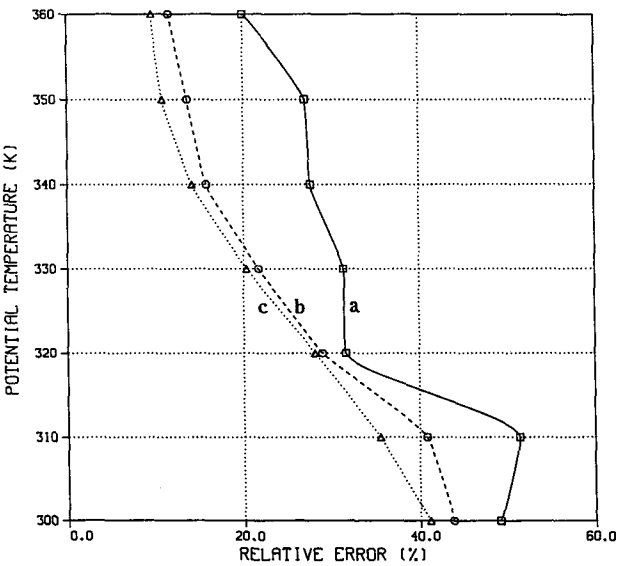

FIG. 7. Same as Fig. 5 but where the reference stability factor is extracted using only 10 pressure levels.

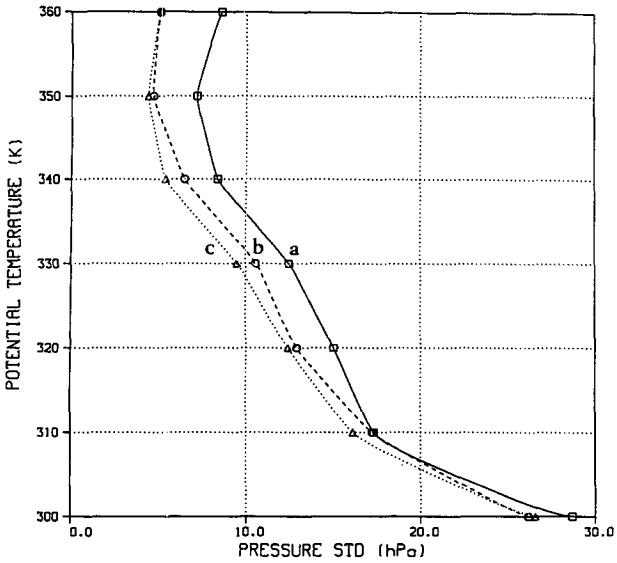

FIG. 8. Standard deviation of the pressure derived by methods (a) (solid), (b) (dashed), and (c) (dotted) for the 100 sondes' output using data from seven pressure levels relative to reference values extracted from observations.

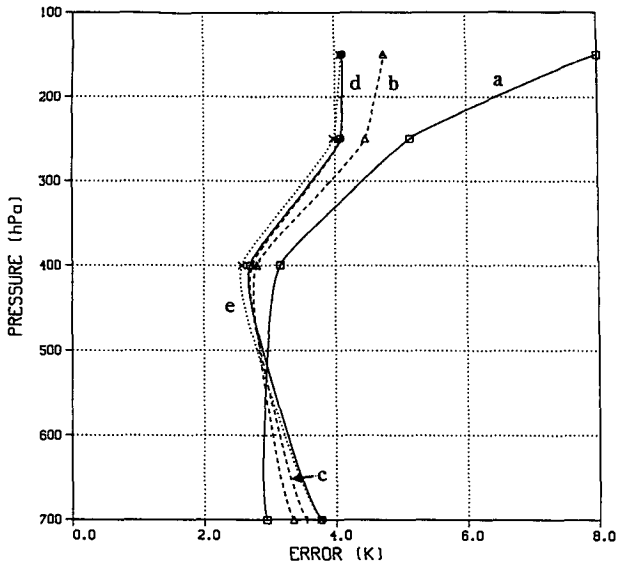

FIG. 9. Standard deviation of potential temperature interpolated from pressure levels 850, 500, 300, 200, and 100 hPa by methods (a) and (d) (solid), methods (b) and (c) (dashed), and method (e) (dotted).

vertical profiles. In order to verify their hierarchy, they were applied using 850-, 500-, 300-, 200-, and 100-hPa data for calculation of potential temperature at the intermediate pressure levels 700, 400, 250, and 150 hPa. The standard deviation between the calculated and the exact values are shown in Fig. 9. Surprisingly, at the 700-hPa level, method (a) is the best, but from 400 hPa upward it is the worst. Methods (e) and (d) are very close to each other; they are the worst at the 700-hPa level but the best at the other levels. These results are consistent with the above findings, since the relevant isentropic layers correspond to 500 hPa upward.

f. "Acid test"

Another way to compare the interpolation methods is to perform a double transformation, the so-called "acid test" (Shen et al. 1986). The interpolation methods were applied, using 10-pressure-level data, to calculate the pressure [and for method (d) also the geopotential height] at 13 isentropic levels ranging from 300 to 360 K with 5-K interval and then back to the original pressure levels, calculating the potential temperature. The standard deviations of the calculated from the exact values for all of the five methods are shown in Fig. 10. Method (a) is the worst, except for 700 hPa, where method (b) is the worst. Method (d) is the best and is very close to method (e). Other acid tests were done for lower resolutions in potential temperature and in pressure separately, and showed the same hierarchy among the interpolation methods, though with larger errors. The errors increased when the resolutions of either θ or p were reduced.

5. Visual comparison of methods (a) and (d)

A practical way to compare two interpolation methods is by visualizing the pertinent PV distributions. Figure 11 shows the PV distributions for the same case shown in Fig. 2 but with the use of method (d), which was found to be the best by the quantitative study. Comparison between Figs. 11 and 2 reveals some im-

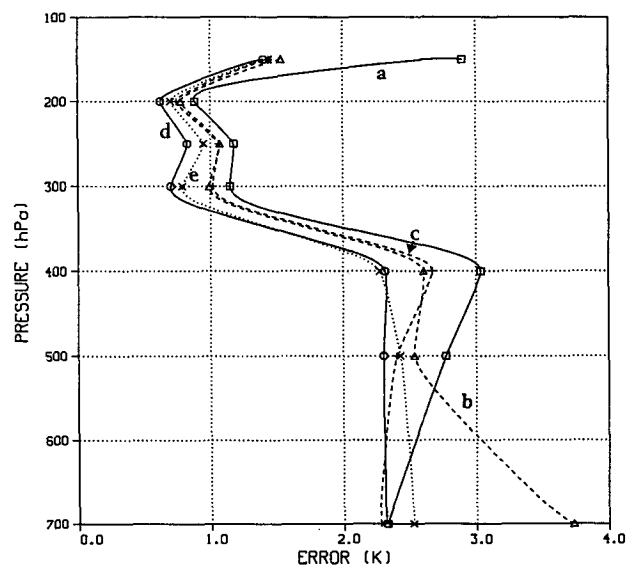

FIG. 10. Standard deviation of potential temperature calculated at pressure levels by double transformation (acid test) from the exact values by methods (a) and (d) (solid), methods (b) and (c) (dashed), and method (e) (dotted).

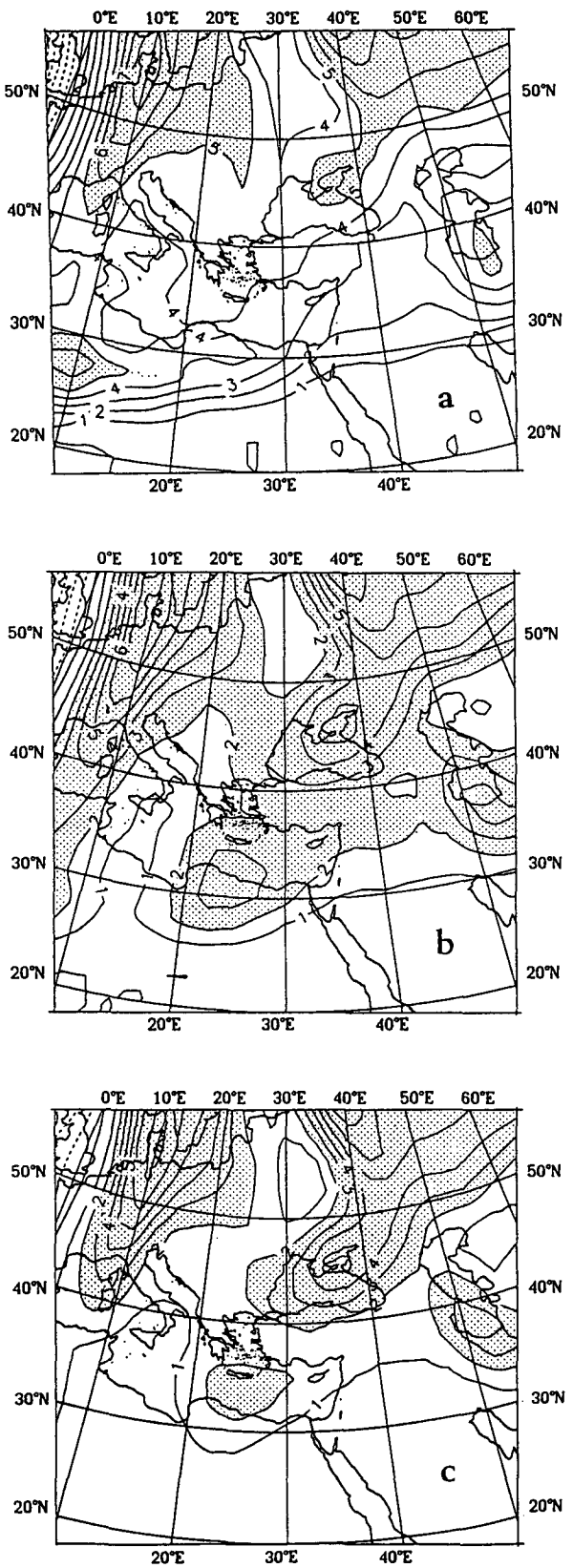

FIG. 11. Same as Fig. 2 but for PV derived by method (d).

portant differences. The isentropic PV distributions obtained by method (d) are quite self-consistent (Figs. 11a–c) in contrast with those obtained by method (a) (Figs. 2a–c). Vertical cross sections through the regions where substantial inconsistencies between adjacent isentropic surfaces in the PV field exist are drawn in Fig. 12. Figures 12a–c show the three vertical PV cross sections for the same case shown in Fig. 2 as derived by method (a), while Figs. 12a′–c′ follow method (d). Since in the region shown in Figs. 2 and 11 the PV increases monotonically with height, a positive PV anomaly is expressed in the vertical cross section by concave PV isolines, and a negative anomaly by convex isolines. Inconsistency in the PV anomalies structure is expressed by a situation in which concave (convex) PV isolines lie above convex (concave) ones. The vertical heavy lines shown in the different cross sections denote regions where such inconsistencies exist. In cases where the PV was derived by method (a), this is clearly pronounced (left panel). For example, the line drawn in Fig. 12c indicates positive anomaly at the 350-K isentropic level, just above a negative anomaly at 340 K, while a pronounced positive anomaly is found at the lower levels. This inconsistency is not observed at the corresponding cross section where the PV field is extracted by the use of method (d) (right panel). There, the PV is anomalously positive throughout the different isentropic surfaces. Another example is shown in Fig. 12b, where a positive PV anomaly at the 360-K isentropic level coincides with a pronounced negative anomaly at the 340-K isentropic level and again with a major positive anomaly at the lower levels. Here also the distribution of PV, when derived by method (d), is more continuous. Most of the relevant region is characterized by a major positive anomaly, while the negative above-mentioned anomaly has only a minor signature.

Corresponding vertical cross sections derived by the use of methods (c) and (e) are very similar to these derived by method (d), whereas those following method (b) are as smooth as method (d), though the features are slightly closer to these seen in the cross sections derived by method (a). A parallel comparison (not shown) made for vertical cross sections with a vertical resolution of 5 K shows similar differences between the interpolation methods.

6. Summary

Five interpolation methods for conversion of data from discrete pressure levels to isentropic levels are compared. The quantitative part deals with the local θ–p relationship and the stability factor by the use of radiosonde data and the illustrative part concentrates on PV distributions derived from initialized ECMWF data. The five methods differ by the T–p functional relationship assumed to hold between adjacent pressure levels as follows. Method (a) assumes linear depen-

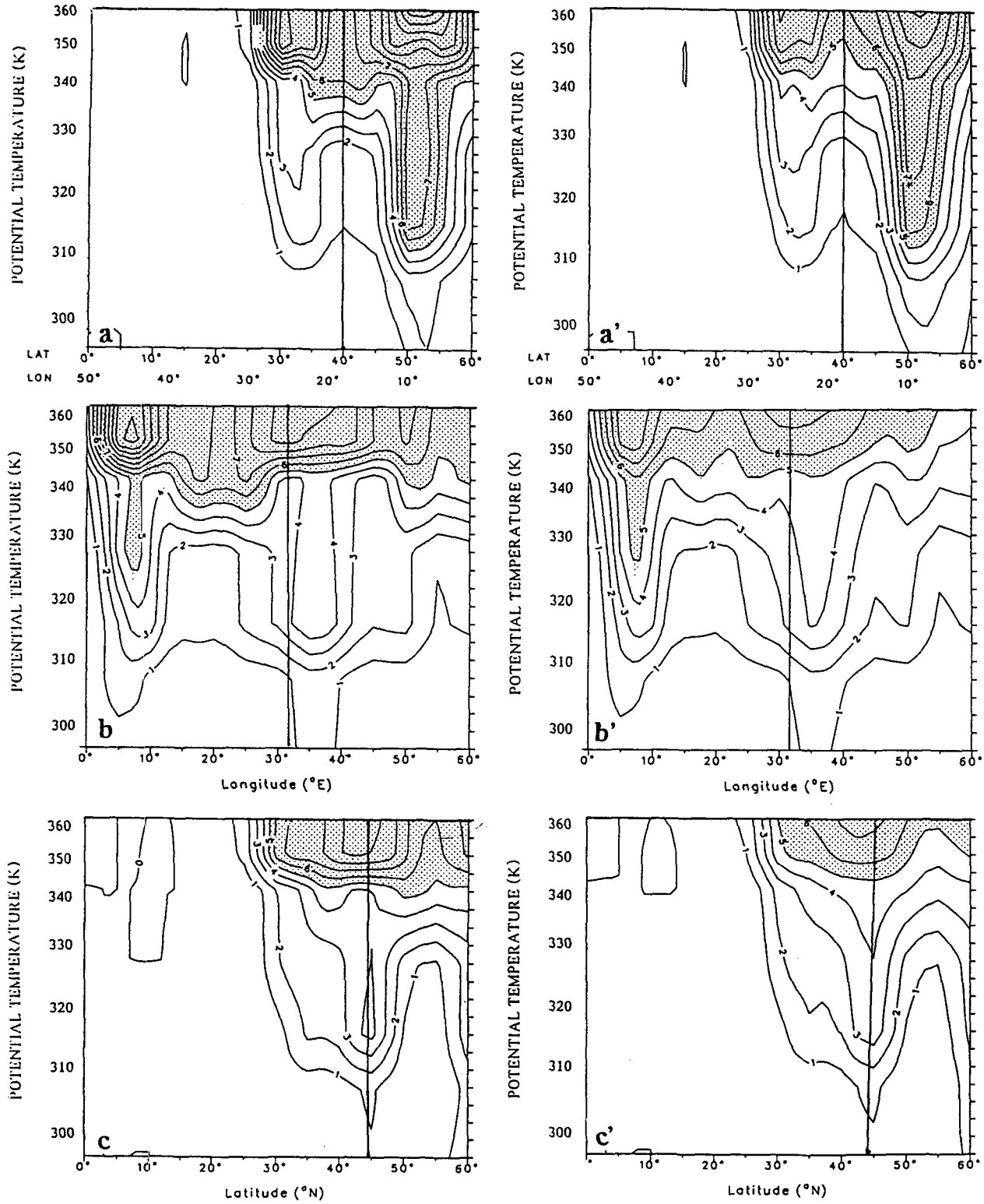

FIG. 12. Vertical distribution of PV for the same case shown in Figs. 2 and 11 with 1-PVU interval. Values exceeding 5 PVU are shaded. The cross sections are made along the heavy lines denoted *A* [for (a) and (a)], *B* [for (b) and (b')], and *C* [for (c) and (c')] shown in Fig. 2. Cross sections (a)–(c) are done with method (a) (left panel), while cross sections (a')–(c') are with method (d) (right panel).

dence of potential temperature on *pressure* p, while method (b) assumes linear dependence on the *Exner function,* or p^{κ}. In method (c) a linear dependence of temperature on the *log pressure* $\ln p$ is assumed. Method (d) assumes a constant lapse rate, say that temperature depends linearly on *height.* The last method, (e), assumes linear dependence of temperature on p^{κ}.

The quantitative study indicates that none of the methods, when using 7 pressure levels, is capable of resolving the fine detailed vertical structure of the stability factor better than to an accuracy of 30%–70%. When interpolating from 10 pressure levels the error is reduced to only 30%–50%. Application of method (c)–(e) to 7-pressure-level data yields better correspondence between the profile of the stability factor and the profile based on 10 pressure levels, where the errors are reduced to 10%–40%. Other comparative tests showed a consistent hierarchy among the interpolation methods. Method (a) is the worst, while methods (c)–(e) are the best, with no significant differences among them.

A comparison among PV charts derived using the interpolation methods shows that all of the methods are capable of capturing the major synoptic-scale features. However, the superiority of methods (c)–(e) over method (a) is clearly seen here as well. The PV anomalies' structure, when derived by method (a), is shown to be discontinuous with height, and such discrepancies disappear when the PV is derived through methods (c)–(e) and only in part with method (b). Currently, mathematical devices, such as Lagrange polynomials (e.g., Shen et al. 1986), are used to achieve smooth and consistent field distributions. Here it is shown that this can be achieved when the interpolation is based on a proper functional T–p relationship.

The small differences between methods (c), (d), and (e), that is, the PV error insensitivity, may be attributed to the affinity of the T–p relationship assumed. Linear T–$\ln p$ [method (c)] relation is the expansion of linear T–z relation [method (d)] in $\ln p$ up to first order (Shen et al. 1986). The affinity between methods (c) and (e) may be explained by the close functional relationship of $\ln p$ and $p^{0.286}$, which are assumed to vary linearly with T for the corresponding methods.

The above findings lead to some practical conclusions. Any quantitative study dealing with PV and using low-resolution pressure data may suffer from severe inaccuracies. When higher-resolution data are used, such as mesoscale model output, methods (c)–(e) are recommended. For synoptic purposes, all of the five methods are capable of displaying the main features, but even here, methods (c)–(e) are doing better. The errors decrease significantly as the resolution of the pressure data is improved. The resolution of isentropic levels has no impact on the PV error, unless data is to be converted back into pressure levels.

Acknowledgments. We thank the German Israeli Foundation (GIF) Grant I-138-120.8/89 for supporting this research. Thanks to ECMWF for the data and to Prof. J. Egger and Dr. A. Tafferner for valuable discussions and for the sonde data. Thanks to the anonymous reviewers for their helpful comments.

REFERENCES

Bengtsson, L., M. Kanamitsu, P. Kollberg, and S. Uppala, 1982: FGGE 4-dimensional data assimilation at ECMWF. *Bull. Amer. Meteor. Soc.,* **63,** 29–43.

Bleck, R., 1973: Numerical forecasting experiments based on the conservation of potential vorticity on isentropic surfaces. *J. Appl. Meteor.,* **12,** 737–752.

——, 1974: Short range prediction in isentropic coordinates with filtered and unfiltered numerical models. *Mon. Wea. Rev.,* **102,** 813–829.

Davis, C. A., and K. A. Emanuel, 1991: Potential vorticity diagnostics of cyclogenesis. *Mon. Wea. Rev.,* **119,** 1929–1953.

Hoerling, M. P., and L. L. Sanford, 1993: On the uncertainty in estimates of atmospheric heating due to data post processing. *J. Climate,* **6,** 168–174.

Hollingsworth, A., D. B. Shaw, P. Lönnberg, L. Illari, K. Arpe, and A. J. Simmons, 1986: Monitoring of observations and analysis quality by a data assimilation system. *Mon. Wea. Rev.,* **114,** 861–879.

Holton, J. R., 1992: *An Introduction to Dynamic Meteorology.* 3d ed. Academic Press., 511 pp.

Hoskins, B. J., M. E. McIntyre, and A. W. Robertson, 1985: On the use and significance of isentropic potential vorticity maps. *Quart. J. Roy. Meteor. Soc.,* **111,** 877–946.

Houghton, D. D., 1985: *Handbook of Applied Meteorology.* John Wiley & Sons Inc., 1461 pp.

Neeman, B. U., and P. Alpert, 1990: Visualizing atmospheric fields on a personal computer: Application of potential vorticity analysis. *Bull. Amer. Meteor. Soc.,* **71,** 154–160.

Schaack, T. K., D. R. Johnson, and M. Wei, 1990: The three-dimensional distribution of atmospheric heating during the GWE. *Tellus,* **42A,** 305–327.

Shaw, D. B., P. Lönnberg, A. Hollingworth, and P. Under, 1987: Data assimilation: The 1984/85 revision of the ECMWF mass and wind analysis. *Quart. J. Roy. Meteor. Soc.,* **113,** 533–566.

Shen, R., E. R. Reiter, and J. F. Bresch, 1986: Vertical interpolation of meteorological variables. *Mon. Wea. Rev.,* **114,** 123–134.

WMO, 1988: Manual on Codes. Vol. 1, Part A, Publication 306, World Meteorological Organization, 245 pp.